Title
Convective heat transfer in planetary dynamo models

Permalink
https://escholarship.org/uc/item/4ms8b9ng

Journal
Geochemistry Geophysics Geosystems, 11(6)

ISSN
1525-2027

Authors
King, Eric M
Soderlund, Krista M
Christensen, Ulrich R
et al.

Publication Date
2010-06-01

DOI
10.1029/2010gc003053

Peer reviewed

Click Here for Full Article

Convective heat transfer in planetary dynamo models

Eric M. King and Krista M. Soderlund

Department of Earth and Space Sciences, University of California, Los Angeles, California 90095–1567, USA
(eric.king@ucla.edu)

Ulrich R. Christensen and Johannes Wicht

Max–Planck–Institut für Sonnensystemforschung, D–37191 Katlenburg–Lindau, Germany

Jonathan M. Aurnou

Department of Earth and Space Sciences, University of California, Los Angeles, California 90095–1567, USA

[1] The magnetic fields of planets and stars are generated by the motions of electrically conducting fluids within them. These fluid motions are thought to be driven by convective processes, as internal heat is transported outward. The efficiency with which heat is transferred by convection is integral in understanding dynamo processes. Several heat transfer scaling laws have been proposed, but the range of parameter space to which they apply has not been firmly established. Following the plane layer convection study by King et al. (2009), we explore a broad range of buoyancy forcing (Ra) and rotation strength (E^{-1}) to show that heat transfer (Nu) in spherical dynamo simulations occurs in two distinct regimes. We argue that heat transfer scales as $Nu \sim Ra^{6/5}$ in the rapidly rotating regime and $Nu \sim Ra^{2/7}$ in the weakly rotating regime. The transition between these two regimes is controlled by the competition between the thermal and viscous boundary layers. Boundary layer scaling theory allows us to predict that the transition between the regimes occurs at a transitional Rayleigh number, $Ra_t = E^{-7/4}$. Furthermore, boundary layer control of heat transfer is shown to relate to the interior temperature profiles of the models. In the weakly rotating regime, the interior fluid is nearly adiabatic. In the rapidly rotating regime, adverse mean temperature gradients abide, irrespective of the Reynolds number (Re). Extrapolating our results to Earth's core, we estimate that core convection resides in the rapidly rotating regime, with $Ra \approx 2 \times 10^{24}$ ($Ra/Ra_t \approx 0.02$), corresponding to a superadiabatic density variation of $\Delta\rho/\rho_o \approx 10^{-7}$, which is significantly below the sensitivity of present seismic observations.

1. Introduction

[2] Many astrophysical and geophysical bodies contain large quantities of electrically conducting fluids: plasma in the Sun; liquid metal in the cores of Earth and other terrestrial worlds; metallized hydrogen gas in Jupiter and Saturn; and ionic fluids in Uranus and Neptune [*Gubbins and Roberts*, 1987; *Stevenson*, 2003; *Miesch*, 2005]. Motions within these fluids generate electrical current systems that power the magnetic fields we observe on these bodies. The conversion of kinetic energy into electromagnetic energy is known as dynamo action. The kinetic energy needed to fuel dynamo action is widely thought to be driven by convection in Earth's core, within the Sun, as well as within the Giant Planets. Most planetary dynamo models then consist of a spherical shell of conducting fluid, with thermal energy deposited at the inner boundary and extracted from the outer. Unstable to this configuration, the fluid convects to transport heat outward and generates electrical currents that can produce self-sustaining magnetic fields.

[3] Geophysical and astrophysical bodies rotate, and this background rotation acts upon the convecting fluid via the Coriolis force. Rapidly rotating convection tends to produce well-organized, axially aligned flow structures. This organizational effect of the Coriolis force constrains the efficiency of heat transfer [e.g., *Rossby*, 1969; *Liu and Ecke*, 2009] and is thought to permit the generation of large-scale magnetic fields [*Olson and Christensen*, 2006; *Käpylä et al.*, 2009]. When the system is forced with sufficient strength, or when the system rotates sufficiently slowly, convection can break free of the constraints of rotation, and results in more chaotic three dimensional turbulence [*Gilman*, 1977; *Aurnou et al.*, 2007; *King et al.*, 2009]. Such flows have been found to generate smaller-scale magnetic fields [*Kutzner and Christensen*, 2002; *Olson and Christensen*, 2006; *Käpylä et al.*, 2009].

[4] In this paper, we explore the limits of rotational control of convection dynamics in planetary dynamo models via measurements of heat transfer efficiency in 200 numerical dynamos, spanning a broad range of parameter space. In section 2 we briefly review previous work on heat transfer in rotating convection. In section 3 we detail our numerical methodology. In section 4 we present heat transfer results from the dynamo models. In section 5 we discuss interior temperature profiles,

and we apply these results to Earth's core in section 6. Last, a summary is given in section 7.

2. Previous Studies of Rotating Convective Heat Transfer

2.1. Role of Boundary Layers

[5] The nondimensional parameters used in this study are defined in Table 1. The five base input parameters consist of buoyancy forcing, strength of rotation, fluid properties, and shell geometry. The strength of buoyancy forcing versus diffusive effects is characterized by the Rayleigh number, Ra. The strength of the Coriolis force versus viscosity is characterized by the inverse of the Ekman number, E^{-1}. The relative values of the fluid's diffusivities are characterized by the thermal and magnetic Prandtl numbers, Pr and Pm, respectively. The spherical shell geometry is characterized by the ratio between inner and outer radii, χ. The key output parameter used in this study is the Nusselt number, Nu. The Nusselt number characterizes the efficiency of convective heat transfer as the ratio of total (superadiabatic) heat transfer to that transferred by diffusion alone.

[6] Our goal is to describe heat transfer behavior by assessing how Nu depends on the control parameters Ra, E, Pr, and Pm. Studies of nonrotating ($E = \infty$), turbulent convection often seek to fit empirical data with power law scalings of heat transfer efficiency versus thermal driving,

$$Nu \propto Ra^{\alpha}, \tag{1}$$

for a given fluid (fixed Pr, Pm). The influence of rotation adds a new degree of freedom to the system, spreading heat transfer data in two dimensions, Ra and E. The goal of heat transfer scaling analysis is to collapse these heat transfer data. This is typically done by invoking some physically motivated combination of control parameters [e.g., *Boubnov and Golitsyn*, 1990; *Canuto and Dubovikov*, 1998; *Schmitz and Tilgner*, 2009; *Liu and Ecke*, 2009; *King et al.*, 2009]. The comparison between theoretically founded scaling arguments and empirical data therefore allows us to test our understanding of convection dynamics. Furthermore, these scalings permit extrapolation of model behavior to the extreme parameter values of planets and stars, at which models cannot be directly evaluated.

[7] *King et al.* [2009] examine heat transfer behavior in plane layer, nonmagnetic, rotating convection and

Table 1. Typical Nondimensional Parameters Used in Boussinesq Dynamo Models, With Comparative Estimates for Earth's Core[a]

Term	Explanation	Definition	Earth's Core	Dynamo Factory Models	Dynamo Subset
Ra	buoyancy/diffusion	$\alpha_T g_o \Delta T L^3 / \nu \kappa$	$\sim 2 \times 10^{24}$	$3 \times 10^5 \leq Ra \leq 2.2 \times 10^9$	$2 \times 10^6 < Ra < 5 \times 10^8$
E	Coriolis/viscosity	$\nu / 2\Omega L^2$	$\sim 10^{-15}$	$5 \times 10^{-7} \leq E \leq 5 \times 10^{-4}$	$5 \times 10^{-6} \leq E \leq 10^{-4}$
Pr	viscous diffusion/thermal diffusion	ν / κ	$\sim 10^{-1}$	$0.1 \leq Pr \leq 30$	$1 \leq Pr \leq 2$
Pm	viscous diffusion/magnetic diffusion	ν / η	$\sim 10^{-6}$	$0.06 \leq Pm \leq 20$	$1 \leq Pm \leq 2$
χ	radius ratio	R_i / R_o	0.35	0.35	0.40
Nu	total heat flux/conductive heat flux	$qL/k\Delta T$	$\sim 5 \times 10^4$	$1 < Nu < 32$	$2.5 < Nu < 25$
Λ	Lorentz/Coriolis	$\sigma B_o^2 / 2\rho\Omega$	$\sim 10^{-1}$	$0.013 < \Lambda < 150$	$0.14 < \Lambda < 42$
Ra_t	boundary layer crossing	$E^{-7/4}$	$Ra/Ra_t \approx 2 \times 10^{-2}$	$0.013 < Ra/Ra_t < 40$	$0.042 \leq Ra/Ra_t \leq 42$
Re	inertia/viscosity	UL/ν	$\sim 10^8$	$1 < Re < 3 \times 10^3$	$30 < Re < 3 \times 10^3$

[a]Here α_T is the coefficient of thermal expansion, g_o is gravitational acceleration on the outer boundary, ΔT is the (superadiabatic) temperature drop from inner to outer boundary, L is the shell thickness, ν is the viscous diffusivity, κ is the thermal diffusivity, Ω is the background rotation rate, η is magnetic diffusivity, q is the heat flow per unit area, k is the fluid's thermal conductivity, σ is the fluid's electrical conductivity, B_o is the mean magnetic field strength, ρ is the Boussinesq fluid density, and U is the mean fluid velocity. The Nusselt number, Nu, is the ratio between the total and conductive aspects of superadiabatic heat flux.

find two distinct regimes (see Figure 1). In the weakly rotating regime, heat transfer is independent of the rotation rate, and scales as

$$Nu \sim Ra^{2/7}, \qquad (2)$$

similar to power law fits from the wealth of non-rotating convection studies [e.g., *Castaing et al.*, 1989; *Glazier et al.*, 1999]. This scaling is signified by the solid line in Figure 1. In the rapidly rotating regime, heat transfer data exhibits a steeper scaling

behavior. The transition between these two heat transfer regimes is argued to be controlled by the relative thicknesses of the boundary layers. Boundary layers are thin regions of fluid immediately adjacent to the bounding surface where diffusive effects become important. Two boundary layers exist in the rotating convection system: the thermal boundary layer; and the viscous boundary layer, which is the so-called Ekman layer in Coriolis force-dominated systems. *King et al.* [2009]
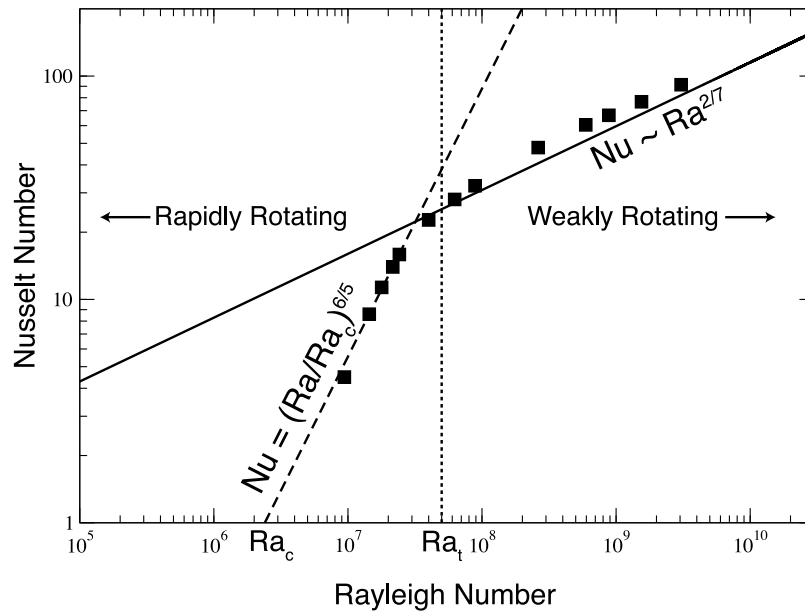

Figure 1. Convective heat transfer data, Nu, versus Ra in a rotating right cylinder of water with $E \approx 4 \times 10^{-5}$ (adapted from *King et al.* [2009]). The dotted vertical line indicates the transitional Rayleigh number, $Ra = Ra_t = E^{-7/4}$. The dashed line represents the rapidly rotating scaling, $Nu = (Ra/Ra_c)^{6/5}$, and the solid line indicates the nonrotating scaling, $Nu \sim Ra^{2/7}$. The rapidly rotating scaling is dependent on $Ra_c \sim E^{-4/3}$, which is the critical Rayleigh number predicting the onset of hydrodynamic convective instability [e.g., *Jones et al.*, 2000].

suggest that when the Ekman layer is thinner than the thermal boundary layer, convective heat transfer is inhibited by the influence of rotation. Conversely, when the thermal boundary layer is thinner, the constraining influence of rotation on convection is lost, and so heat transfer conforms to the nonrotating behavior.

[8] Theoretical scalings of the boundary layer thicknesses permit a prediction of the transition point between the two regimes. The Ekman and thermal boundary layers have thicknesses

$$\delta_E \sim E^{1/2} \quad \text{and} \quad \delta_\kappa \sim Nu^{-1}, \qquad (3)$$

respectively [Greenspan, 1968; Spiegel, 1971]. The transition is predicted to occur where the boundary layers cross, i.e., when $\delta_E = \delta_\kappa$. The Nusselt number at which the transition should occur is then

$$Nu_t \sim E^{-1/2}. \qquad (4)$$

The Nusselt number can be related to the Rayleigh number using the heat transfer scaling law $Nu \sim Ra^{2/7}$. This allows us to solve for the Rayleigh number at which the boundary layers are predicted to cross:

$$Ra_t = E^{-7/4}, \qquad (5)$$

which we call the transitional Rayleigh number. Note that in the work by King et al. [2009], there is a scaling prefactor on the right-hand side of (5) of 1.4. Here we set this prefactor to unity.

[9] We predict a rapidly rotating heat transfer scaling law using the boundary layer controlled transition point. First, we assume a rapidly rotating scaling law of the form $Nu = (Ra/Ra_c)^\gamma$, where Ra_c is the critical Rayleigh number for the onset of convection, $Ra_c \propto E^{-4/3}$ [Chandrasekhar, 1953]. In order for this scaling law to intersect with the weakly rotating power law (2) at the transitional Rayleigh number (5), the rapidly rotating scaling exponent must be $\gamma = 6/5$, yielding

$$Nu = (Ra/Ra_c)^{6/5} \qquad (6)$$

in the rotationally controlled convection regime. This scaling is signified by the dashed line in Figure 1. The introduction of the Coriolis force to this scaling through the critical Rayleigh number signifies the importance of rotation in this regime.

[10] The separation of rotating convection dynamics into rapidly rotating and weakly rotating regimes is not new [e.g., Gilman, 1977; Kutzner and Christensen, 2002; Aurnou et al., 2007; Driscoll and Olson, 2009]. Canuto and Dubovikov [1998], for example, work to distinguish two such regimes based on convective mixing length theory. Christensen and Aubert [2006] and Olson and Christensen [2006] use an a posteriori measurement of a local Rossby number to differentiate the two regimes in terms of magnetic field morphology in dynamo models. Schmitz and Tilgner [2009] separate the two regimes by comparing heat transfer with measurements of a modified Peclet number in plane layer rotating convection simulations. Here we test whether the boundary layer controlled transition predicted by King et al. [2009] adequately describes the transition between these two regimes in planetary dynamo models.

2.2. Relevance to Dynamo Models

[11] We hypothesize that boundary layer control of rotating convective heat transfer regimes applies to planetary dynamo models. There are several reasons why the plane layer results may fail to apply to planetary and stellar dynamos. For instance, the added complexity of a spherical geometry and the additional dynamic influence of the magnetic field via Lorentz forces were not present in the plane layer study.

[12] In spherical geometries, Ekman boundary layers have latitudinally varying thicknesses [Greenspan, 1968]. Here we treat the Ekman layer as a simple linear boundary layer whose mean thickness is given by (3), and do not consider the dependence of this thickness on latitude. Furthermore, rotating convection in spherical shells is capable of driving strong zonal flows [e.g., Christensen, 2002; Heimpel et al., 2005]. Such flows are not typically observed in plane layer convection. Strong shearing in these zonal flows can influence heat transfer from inner to outer boundary [Aurnou et al., 2008]. Despite these possible complications, a meta-analysis by Aurnou [2007] shows that heat transfer scaling behavior may not strongly differ between the plane layer and spherical shell geometries.

[13] The presence of magnetic fields may also call into question the application of the plane layer, hydrodynamic results to dynamo models. For example, in studies with externally imposed magnetic fields, the Lorentz force acts to constrain fluid motions and inhibits heat transfer [Cioni et al., 2000; Aurnou and Olson, 2001]. However, in fully self-consistent dynamo models, heat transfer
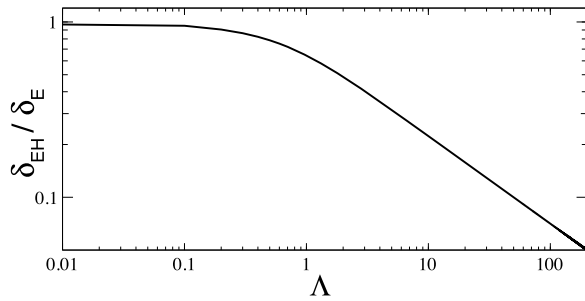
Figure 2. The theoretical Ekman-Hartmann layer thickness normalized by that of the Ekman layer, δ_{EH}/δ_E, as defined by equations (3) and (7), versus the Elsasser number, Λ. The Ekman-Hartmann layer thickness only differs significantly from the Ekman layer thickness in the presence of strong imposed magnetic fields.

scaling behavior is not found to differ significantly from that of comparable models without magnetic fields [*Christensen*, 2002; *Christensen and Aubert*, 2006; *Aurnou*, 2007].

[14] Another complication in applying the results of *King et al.* [2009] to dynamo models is introduced by the fact that the Ekman layer may no longer be an adequate representation of the viscous boundary layer. Instead, flows in the presence of magnetic fields and background rotation produce an Ekman-Hartmann layer [e.g., *Desjardins et al.*, 2001]. This boundary layer balances the viscous force at the bounding surfaces with both Coriolis and Lorentz forces, instead of with the Coriolis force alone as in the case of the Ekman layer. The Ekman-Hartmann layer scales as [*Gilman and Benton*, 1968; *Debnath*, 1973]

$$\delta_{EH} \sim \left[\left(\Lambda^2 + 1 \right)^{1/2} - \Lambda \right]^{1/2} E^{1/2}, \qquad (7)$$

where Λ is the Elsasser number. The Elsasser number characterizes the ratio of the strength of the Lorentz force to that of the Coriolis force, and is defined in Table 1. Figure 2 shows the ratio of the theoretical Ekman-Hartmann layer and Ekman layer thicknesses versus Λ for a uniform imposed transverse magnetic field in a plane fluid layer. The dynamo models presented here have a mean Elsasser number of 7.4, with extrema at $0.01 \lesssim \Lambda \lesssim 150$. Assuming the boundary layer dynamics do not differ between flows with imposed magnetic fields and those with self-generated dynamo fields, Figure 2 illustrates that the thickness of the Ekman-Hartmann layer scales differently than the Ekman layer for the dynamo models with higher Λ values.

Therefore, the development of the transitional Rayleigh number from the nonmagnetic [*King et al.*, 2009] study may not be appropriate for dynamo models.

[15] We also assume that the Rayleigh number at which convection onsets follows the theoretical scaling for rapidly rotating, nonmagnetic convection in a sphere, $Ra_c \propto E^{-4/3}$ [*Roberts*, 1968; *Busse*, 1970; *Jones et al.*, 2000; *Dormy et al.*, 2004]. In the presence of strong imposed magnetic fields ($\Lambda \gtrsim \mathcal{O}(1)$), the critical Rayleigh number has been shown to scale differently, as $Ra_c \propto E^{-1}$ [*Zhang*, 1995; *Fearn*, 1998]. Studies of convection dynamics in the presence of imposed magnetic fields therefore suggest a significant difference from that found in hydrodynamic studies. For example, a critical Rayleigh number difference of $E^{1/3}$ between magnetoconvection and nonmagnetic convection studies predicts an order of magnitude difference in Ra_c across our range of Ekman numbers. Assuming the magnetoconvection results apply to dynamo models, this may again invalidate the scalings given by *King et al.* [2009].

[16] We hypothesize that the boundary layer control of heat transfer regimes demonstrated in the nonmagnetic, plane layer convection study also applies to planetary dynamo models. This hypothesis makes the following two predictions. First, heat transfer occurs in two separate regimes, rapidly rotating and weakly rotating, with distinct empirical heat transfer scalings in each regime, $Nu = (Ra/Ra_c)^{6/5}$ and $Nu \sim Ra^{2/7}$, respectively. Second, the transition between regimes is determined by relative boundary layer thicknesses and is described by the transitional Rayleigh number, $Ra_t = E^{-7/4}$. In this work, we test these predictions using a broad array of numerical dynamo models.

3. Numerical Method

[17] We consider three-dimensional convection of a Boussinesq, electrically conducting fluid in a spherical shell rotating about the axial $\hat{z}$ direction with fixed angular velocity Ω. The shell has isothermal boundaries with an imposed temperature contrast of ΔT between inner and outer boundaries. Absolute temperature values are therefore arbitrary, as the temperature on the outer boundary is set to $T(r = R_o) = 0$ for convenience. Gravity is assumed to vary linearly with radius and has a value of g_o on the outer boundary. Figure 3 shows a schematic depiction of the dynamo model's geometry.
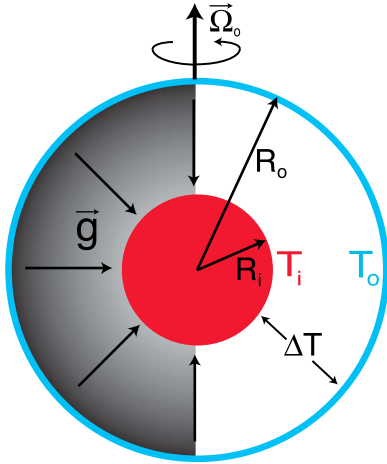
Figure 3. A schematic illustration of the dynamo model geometry. The convecting fluid is contained in a spherical shell between a hot inner boundary and cold outer boundary, $T_i > T_o$. Gravity points radially inward and increases linearly with spherical radius. The rotation axis is vertical with uniform nondimensional rotation rate E^{-1}.

[18] The governing equations for this system are:

$$E\left(\frac{\partial \mathbf{u}}{\partial t} + \mathbf{u} \cdot \nabla \mathbf{u} - \nabla^2 \mathbf{u}\right) + \hat{\mathbf{z}} \times \mathbf{u} + \frac{1}{2}\nabla p = \frac{RaE}{Pr}T\mathbf{r}$$
$$+ \frac{1}{2Pm}(\nabla \times \mathbf{B}) \times \mathbf{B}, \qquad (8)$$

$$\frac{\partial \mathbf{B}}{\partial t} = \nabla \times (\mathbf{u} \times \mathbf{B}) + \frac{1}{Pm}\nabla^2 \mathbf{B}, \qquad (9)$$

$$\frac{\partial T}{\partial t} + \mathbf{u} \cdot \nabla T = \frac{1}{Pr}\nabla^2 T, \qquad (10)$$

$$\nabla \cdot \mathbf{u} = 0, \qquad \nabla \cdot \mathbf{B} = 0, \qquad (11)$$

where $\mathbf{u}$ is the velocity vector, $\mathbf{B}$ is the magnetic induction, T is the temperature, and p is the non-hydrostatic pressure [*Wicht*, 2002]. The equations have been nondimensionalized by shell thickness $L = R_o - R_i$ as length scale, ΔT as temperature scale, $\tau_\nu = L^2\nu^{-1}$ as time scale, νL^{-1} as velocity scale, $\rho\nu\Omega$ as pressure scale, and $\sqrt{\rho\mu\eta\Omega}$ as magnetic induction scale. In these definitions, R_o (R_i) is the outer (inner) shell radius, ν is kinematic viscosity, κ is thermal diffusivity, and η is magnetic diffusivity. As dictated by the Boussinesq approximation, density variations are only considered in the buoyancy term (the first term on the right-hand side of (8)), and the thermal expansion coefficient, α_T, the kinematic viscosity, the thermal diffusivity,

and the magnetic diffusivity are constant [*Spiegel*, 1971]. The nondimensional control parameters Ra, E, Pr, and Pm are defined in Table 1.

[19] Equations (1)–(4) are solved simultaneously for $\mathbf{u}$, p, $\mathbf{B}$, and T using the numerical model MagIC version 3.38 [*Wicht*, 2002]. This code makes use of the pseudospectral method first developed by *Glatzmaier* [1984] with subsequent modifications by *Christensen et al.* [1999] and *Wicht* [2002]. The velocity and magnetic induction vectors are decomposed into poloidal and toroidal scalar potentials, which are expanded in Chebyshev polynomials in the radial direction and in spherical harmonic functions on spherical surfaces. MagIC utilizes mixed implicit and explicit time stepping. The Coriolis and nonlinear terms are treated explicitly using a second-order Adams-Bashforth scheme and the diffusion, pressure, and linear terms are treated implicitly using a Crank-Nicolson time step. The implicit time step can vary over time and is controlled by a modified MHD Courant criterion which accounts for viscous and ohmic damping of short-wavelength Alfvén-type oscillations [*Christensen et al.*, 1999]. This damping helps to stabilize the system and allows the use of a slightly larger numerical time step compared to the unmodified MHD Courant criterion. Hyperdiffusion is used in our most extreme cases to increase numerical stability by damping the small-scale components of the flow and magnetic fields. In these cases, the viscous, thermal, and magnetic diffusivities are multiplied by a factor d of the form

$$d(l) = 1 + A\left(\frac{l + 1 - l_{HD}}{l_{max} + 1 - l_{HD}}\right)^\beta \qquad (12)$$

in the spherical harmonic domain. Here A is the hyperdiffusion amplitude, l is the spherical harmonic degree, l_{HD} is the degree above which hyperdiffusion starts to act, l_{max} is the maximum harmonic degree, and β is the hyperdiffusion exponent.

[20] We analyze a data set consisting of twenty-one new simulations, hereon called the dynamo subset models; and one hundred seventy nine additional dynamos referred to as the dynamo factory models, most of which were previously reported by *Christensen and Aubert* [2006], *Olson and Christensen* [2006], and *Christensen et al.* [2009]. To our knowledge, this is the broadest array of planetary dynamo models currently available. The range of parameters explored by each is given in Table 1, and Table 2 details each dynamo

Table 2. Input and Output Parameters for the Dynamo Subset Models[a]

Case	Ra/Ra_t	Ra	E	Pr	Pm	σ_{OC}^{IC}	N_{ro}	N_{ri}	l_{max}	D	l_{HD}	β	Nu	Re	$\langle T \rangle$
	0.04	8.04×10^7	5×10^{-6}	1	1	1	65	25	128	-	-	-	3.60	114	0.276
A	0.14	4.76×10^6	5×10^{-5}	1	2	1	41	17	128	-	-	-	2.64	59	0.257
	0.14	4.76×10^6	5×10^{-5}	2	1	1	41	17	128	-	-	-	2.66	36	0.245
	0.21	2.12×10^6	1×10^{-4}	1	2	1	41	17	64	-	-	-	2.54	52	0.244
	0.28	2.83×10^6	1×10^{-4}	1	2	1	41	17	64	-	-	-	3.18	71	0.237
	0.35	3.54×10^6	1×10^{-4}	1	2	1	41	17	64	-	-	-	3.78	91	0.229
	0.36	3.68×10^6	1×10^{-4}	1	2	1	41	17	64	-	-	-	3.88	95	0.227
	0.37	3.75×10^6	1×10^{-4}	1	2	1	41	17	64	-	-	-	3.94	98	0.225
	0.38	3.82×10^6	1×10^{-4}	1	2	1	41	17	64	-	-	-	4.03	124	0.223
	0.39	3.96×10^6	1×10^{-4}	1	2	1	41	17	64	-	-	-	4.16	127	0.219
	0.41	4.11×10^6	1×10^{-4}	1	2	1	41	17	64	-	-	-	4.28	131	0.221
B	0.42	4.24×10^6	1×10^{-4}	1	2	1	41	17	85	-	-	-	4.38	135	0.217
	0.85	8.50×10^6	1×10^{-4}	1	2	1	41	17	128	-	-	-	6.72	216	0.193
C	1.42	1.42×10^7	1×10^{-4}	1	1	1	49	17	192	-	-	-	8.50	340	0.189
IIC	1.42	1.42×10^7	1×10^{-4}	1	1	0	49	17	192	-	-	-	8.52	341	0.191
H0	2.10	2.10×10^7	1×10^{-4}	1	1	1	49	17	192	-	-	-	9.87	432	0.192
H1	2.10	2.10×10^7	1×10^{-4}	1	1	1	49	17	192	10	25	2	9.89	420	0.191
	4.24	4.24×10^7	1×10^{-4}	1	1	1	49	17	192	-	-	-	12.62	642	0.180
	14.2	1.42×10^8	1×10^{-4}	1	1	1	65	17	192	5	75	2	17.90	1239	0.162
	14.2	4.76×10^8	5×10^{-5}	1	1	1	65	17	192	10	20	2	24.18	1981	0.174
D	42.4	4.24×10^8	1×10^{-4}	1	1	1	65	17	192	10	25	2	23.42	2113	0.162

[a]The ratio of the inner to outer core electrical conductivities is denoted σ_{OC}^{IC}. The number of radial grid points in the outer and inner cores is denoted N_{ro} and N_{ri}, respectively. The maximum spherical harmonic degree is denoted l_{max}. The hyperdiffusion amplitude, the harmonic degree where hyperdiffusion begins to act, and the hyperdiffusion exponent are A, l_{HD}, and β, respectively. Values in column 16, $\langle T \rangle$, are mean shell temperature calculations discussed in section 5. All other parameters are defined in Table 1. Cases A, B, C, and D are shown in detail in Figures 8 and 9. Cases C, IIC, H0, and H1 are specifically discussed in section 3.

subset case, for which we have more comprehensive diagnostic capabilities. All simulations have an Earth core-like geometry ($\chi \equiv R_i/R_o = 0.4$ for dynamo subset models, and $\chi = 0.35$ for dynamo factory models) and rigid, no-slip, isothermal boundary conditions. The dynamo subset cases are full-sphere calculations with no presumed symmetries.

[21] The inner spheres of the models are either electrically insulating or have the same electrical conductivity as the outer fluid shell. The ratio of conductivities between the two regions in the dynamo subset is unity with one exception to test the importance of inner core conductivity. Cases C and IIC in Table 2 have identical input parameters but with conducting and insulating inner cores, respectively. The Nusselt numbers differ only by about 0.2%, so we can conclude that the inner core conductivity minimally effects the heat transfer behavior.

[22] The four most strongly driven subset cases use hyperdiffusion. For example, case H1 has $A = 10$, $l_{HD} = 25$, $\beta = 2$, $l_{max} = 192$, such that hyperdiffusion acts on spherical harmonic degrees above 25, increasing quadratically with degree. We test its influence by comparing two cases, with and without hyperdiffusion (cases H0 and H1, respectively,

in Table 2). The efficiency of convective heat transfer (Nu) agrees within 0.2% between these two cases.

4. Analysis of Heat Transfer in Dynamo Models

4.1. Testing the Boundary Layer Control Hypothesis

[23] Figure 4 shows heat transfer data, Nu versus Ra, for all dynamo cases. The basic behavior of the heat transfer data are similar to that observed in plane layer studies [e.g., *Rossby*, 1969; *King et al.*, 2009; *Schmitz and Tilgner*, 2009]. Convective heat transfer is strongly affected by the background rotation, whose strength is characterized by E^{-1}. The stabilizing influence of the Coriolis force requires models with higher rotation rates to be driven harder in order to convect [*Chandrasekhar*, 1953]. Thus, the onset of convection is delayed by the influence of rotation as E decreases. As in Figure 1, the heat transfer data follows two basic scaling behaviors. For sufficiently low E and Ra, the data appear to follow the rapidly rotating $Nu \propto Ra^{6/5}$ scaling (dashed line). In contrast, cases with higher E and Ra appear to transition to a weakly rotating $Nu \sim Ra^{2/7}$ scaling (solid line). Thus,
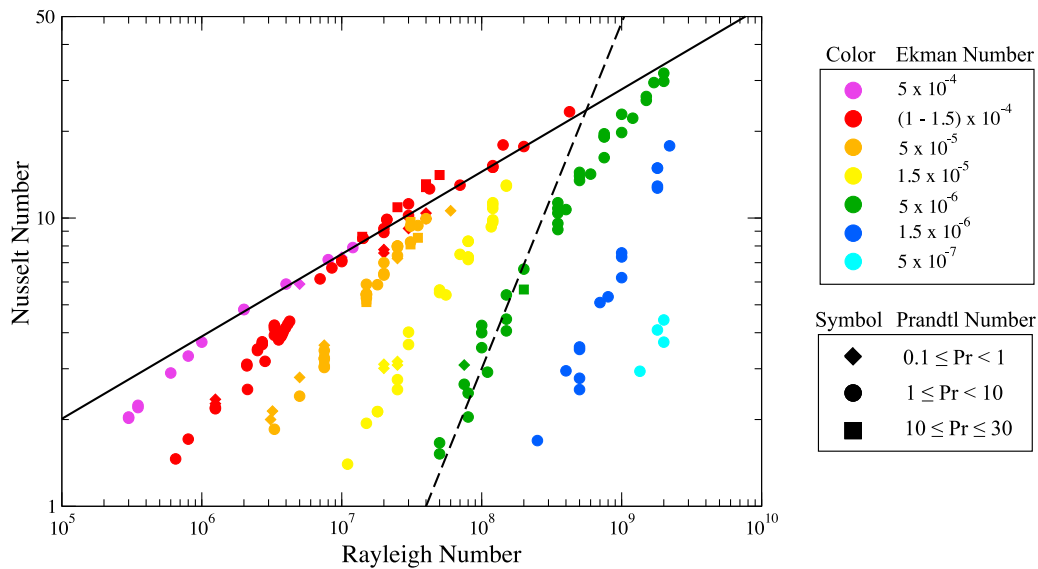
Figure 4. Heat transfer behavior, Nu versus Ra, in planetary dynamo models (dynamo factory and subset models). See Table 1 for parameter ranges. The nonrotating scaling, $Nu_{\text{nonrotating}} = 0.075 Ra^{2/7}$, is shown as a solid line. The rapidly rotating scaling, $Nu \propto Ra^{6/5}$, is shown as a dashed line.

within particular parameter ranges, the data are described by either the rapidly rotating or nonrotating scaling exponents found in the plane layer study (Figure 1).

[24] We aim to collapse the data in Figure 4 through a combination of control parameters. Figure 5 shows Nu normalized by the nonrotating scaling ($Ra^{2/7}$) versus Ra normalized by its predicted transitional value, $Ra_t = E^{-7/4}$, for all dynamo cases. The boundary layer transition scaling effectively collapses the broad array of dynamo heat transfer data. The scaling regimes hinted at by Figure 4 are more clearly observed in this parameter space defined by the boundary layer controlled transitional Rayleigh number.

[25] Well into the rapidly rotating regime ($Ra \lesssim 0.1 Ra_t$), heat transfer behavior are reasonably well described by the $Nu = (Ra/Ra_c)^{6/5}$ scaling (dashed line, (6)). In the weakly rotating regime ($Ra \gtrsim Ra_t$), heat transfer transitions to a $Nu \sim Ra^{2/7}$ scaling (solid horizontal line). A transitional region appears between the two scaling regimes, roughly in the range $0.1 \lesssim Ra/Ra_t \lesssim 2$.

[26] Despite the added complexities of the spherical geometry and magnetohydrodynamic effects, the heat transfer regimes identified in plane layer, nonmagnetic convection (Figure 1) are also evident in these planetary dynamo models (Figures 4 and 5). The collapse of our data using Ra_t shows no strong dependence on the Prandtl numbers, Pr and Pm. Furthermore, our description of the heat transfer

behavior in these dynamo models lacks any explicit dependence on the magnetic field strength; Ra_t and Ra_c depend on the rotation rate, but are independent of magnetic field intensity. Notably, this independence is at odds with studies of rotating convection of in the presence of imposed magnetic fields [e.g., *Chandrasekhar*, 1954; *Nakagawa*, 1959; *Eltayeb and Roberts*, 1970; *Zhang*, 1995; *Aurnou and Olson*, 2001; *Fearn*, 1998].

[27] In order to compare the heat transfer transition to the boundary layers themselves, Figure 6 shows the velocity and thermal boundary layer thicknesses from the dynamo subset models plotted versus the transition parameter, Ra/Ra_t. The velocity boundary layer thickness is defined as the radial location of the first local maximum in RMS velocity above (below) the model's inner (outer) boundary [*Belmonte et al.*, 1994; *King et al.*, 2009]. Similarly, the thermal boundary layer is defined as the radial location of the first local maximum in temperature variance away from the model's boundaries [*Belmonte et al.*, 1994; *King et al.*, 2009]. The influence of magnetic fields does not affect our evaluation of the velocity boundary layer thicknesses, which are calculated directly from the velocity field in each subset case. Figure 6 shows that the two boundary layers cross where $Ra \approx Ra_t$. Thus, the transition from rapidly rotating to weakly rotating heat transfer behavior in the dynamo subset models corresponds well with the interchanging of the two nested boundary layers.
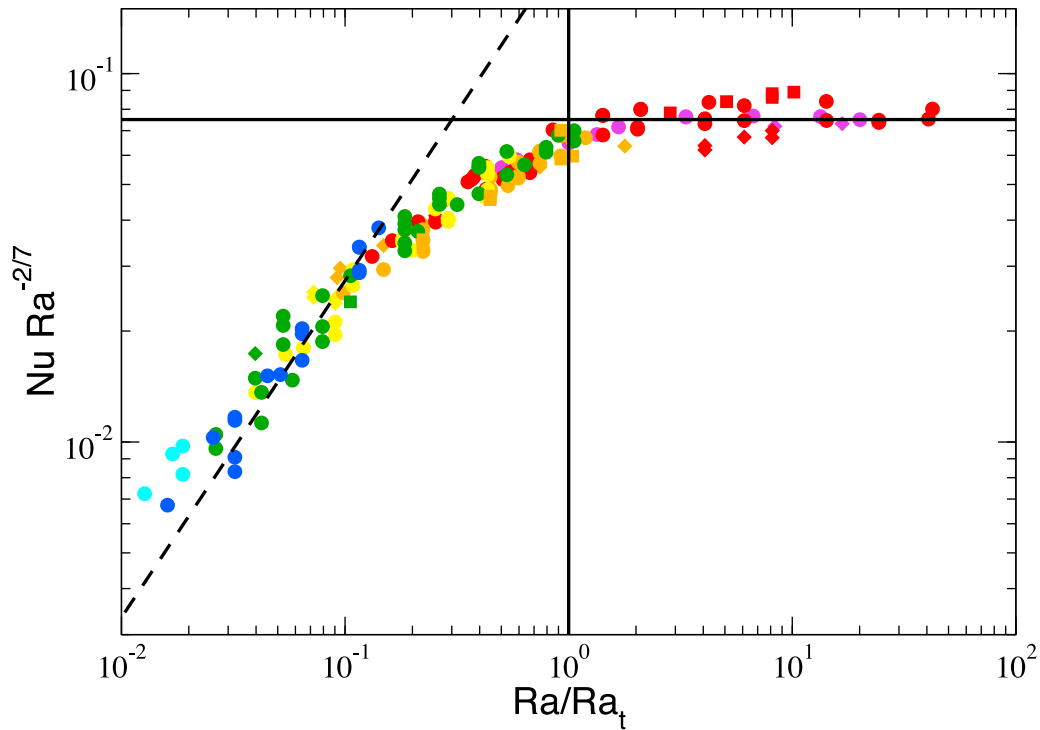
Figure 5. Rescaled heat transfer data from planetary dynamo models (dynamo factory and subset models). Symbols are the same as in Figure 4. The Nusselt number is normalized by the nonrotating scaling, $NuRa^{-2/7}$, and the Rayleigh number is normalized by the transitional Rayleigh number, $Ra/Ra_t = RaE^{7/4}$. The solid horizontal line represents the weakly rotating $Nu = 0.075Ra^{2/7}$ scaling. The dashed line represents the rapidly rotating scaling (14), derived from $Nu = (Ra/Ra_c)^{6/5}$ with $Ra_c \propto E^{-4/3}$.

4.2. Asymptotic Scalings

[28] Boundary layer control of heat transfer behavior in planetary dynamo models allows us to predict the limits of applicability of the various heat transfer scaling laws. In the weakly rotating regime, $Ra > Ra_t$, the data conform to a
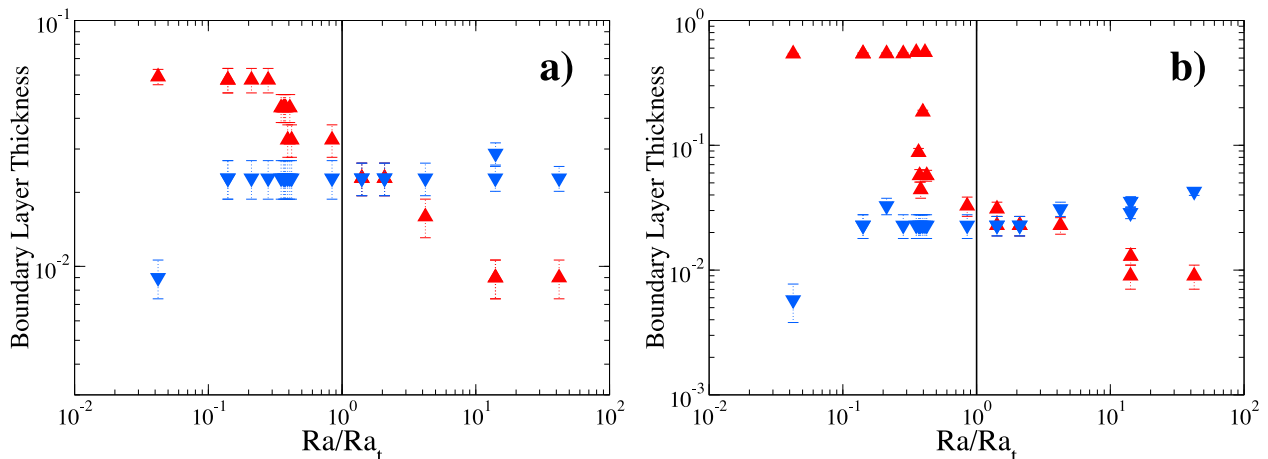
$$Nu = 0.075Ra^{2/7} \qquad (13)$$

Figure 6. Boundary layer thicknesses versus the transition parameter Ra/Ra_t from the dynamo subset on the (a) inner boundary and (b) outer boundary. The velocity boundary layer (an Ekman-Hartmann layer) thickness is shown as downward pointing blue triangles, and the thermal boundary layer is shown as upward pointing red triangles. Boundary layer thicknesses are normalized by the shell thickness, $L = R_o - R_i$. The distance between error bars represents the local spatial resolution. The two boundary layers cross near $Ra = Ra_t$, as predicted.

scaling, a result that is important for the convective regions of slowly rotating stars and planets [e.g., *Palacios et al.*, 2006; *Aurnou et al.*, 2007]. This result also implies that nonrotating, turbulent convective heat transfer may follow a $\alpha \approx 2/7$ scaling in the spherical geometry, like that found in plane layer convection [e.g., *Castaing et al.*, 1989; *Glazier et al.*, 1999]. Nonrotating, plane layer convection has the advantage of being carried out both numerically and in the laboratory. Laboratory convection studies are historically capable of achieving higher degrees of supercriticality than numerical models [e.g., *Niemela et al.*, 2000]. However, high Rayleigh number, nonrotating convection has not been well explored in spherical geometries because of the difficulty in producing a spherically radial gravity field in the laboratory [cf. *Tilgner*, 1996]. The weakly rotating, heat transfer scaling prefactor in the spherical geometry, 0.075, although not well constrained, is lower than that found in the plane layer studies, 0.16. This difference likely is due to geometric effects.

[29] In the rapidly rotating regime, $Ra \lesssim Ra_t$, heat transfer data are fairly well described by the $Nu = (Ra/Ra_c)^{6/5}$ scaling law (6). Assuming $Ra_c = C_1 E^{-4/3}$ [*Jones et al.*, 2000; *Dormy et al.*, 2004], this scaling can be rewritten in terms of the axis parameters in Figure 5 as

$$NuRa^{-2/7} = (Ra/Ra_c)^{6/5}Ra^{-2/7} = C_1^{-6/5}Ra^{32/35}E^{8/5}$$
$$= C_2(Ra/Ra_t)^{32/35}, \qquad (14)$$

which is represented by the dashed line in Figure 5. The scaling prefactor C_2 is determined by fitting the $NuRa^{-2/7} = C_2(Ra/Ra_t)^{32/35}$ scaling to the dynamo data, yielding $C_2 \simeq 0.225$ and thus $C_1 = C_2^{-5/6} \simeq 3.5$. This determination of C_1 is empirical and based on the assumptions that $Nu = (Ra/Ra_c)^{6/5}$ in the rapidly rotating regime with $Ra_c = C_1 E^{-4/3}$. We can compare the prefactor C_1 to theoretical values from *Jones et al.* [2000], who find $1 \lesssim C_1 \lesssim 8$ for $0.1 \leq Pr \leq 10$. Thus, although we ignore the Prandtl number dependence of the critical Rayleigh number, the empirically determined prefactor $C_1 = 3.5$ is in first-order agreement with that from the theoretical, asymptotic analysis of rotating convection.

[30] Previous work by Christensen and coworkers developed a separate heat transfer scaling formulation for rotating convection and dynamo models [*Christensen*, 2002; *Christensen and Aubert*, 2006]. These scalings are independent of molecular diffusivities following Kolmogorov's second hypothesis of similarity [*Kolmogorov*, 1941]. The authors use the rotation period as the dominant time scale to develop diffusivity-free parameters

$$Ra_Q^* = RaNuE^3Pr^{-2} \quad \text{and} \quad Nu^* = NuEPr^{-1}, \qquad (15)$$

and seek a scaling

$$Nu^* \propto Ra_Q^{*\beta}. \qquad (16)$$

Empirically, they find $\beta \approx 6/11$ [*Christensen*, 2002; *Christensen and Aubert*, 2006; *Aurnou*, 2007]. The range of parameter space in which the rotational time scale should be dominant is not quantified, however, and so the applicability of the diffusivity-free scaling is not well bounded.

[31] Figure 7 compares the goodness of fit of the diffusivity free scaling law with that of the rapidly rotating scaling (6) discussed above. The rapidly rotating scaling law (6) and the diffusivity free scaling law (16) can be rewritten in terms of base parameters as

$$Nu = (Ra/Ra_c)^{6/5} \quad \rightarrow \quad Nu \propto Ra^{1.2}E^{1.6}, \qquad (17)$$

$$Nu^* \propto Ra_Q^{*6/11} \quad \rightarrow \quad Nu \propto Ra^{1.2}E^{1.4}Pr^{-0.2}, \qquad (18)$$

respectively. Figure 7 shows heat transfer data from the dynamo models normalized by the two scalings given in (17) and (18). Rather than spreading the data across many orders of magnitude, as in $Nu^*-Ra^*_Q$ plots, here we collapse the data to illustrate the limits of the scaling laws' applicability. The rapidly rotating scaling (17) appears to collapse heat transfer data more effectively than the diffusivity free scaling (18). However, the lack of any clear convergence to a single scaling behavior in Figure 7a (for $Ra < Ra_t$) illustrates that no unambiguous asymptotic behavior has been reached in the rapidly rotating regime.

[32] This ambiguity in asymptotic behavior arises from the limited range of Rayleigh numbers currently accessible within the rapidly rotating regime ($Ra_c < Ra < Ra_t$). A significantly broader range of supercritical ($Ra > Ra_c$), subtransitional ($Ra < Ra_t$) Rayleigh numbers is needed to test the validity of this scaling. The breadth of Rayleigh number accessibility within the rapidly rotating regime scales with the Ekman number as

$$Ra_t/Ra_c \approx \frac{E^{-5/12}}{3.5}. \qquad (19)$$

For example, at an Ekman number of 10^{-5}, the range of Ra within the rapidly rotating regime is only $Ra_t/Ra_c \approx 35$. Thus, in order to produce a
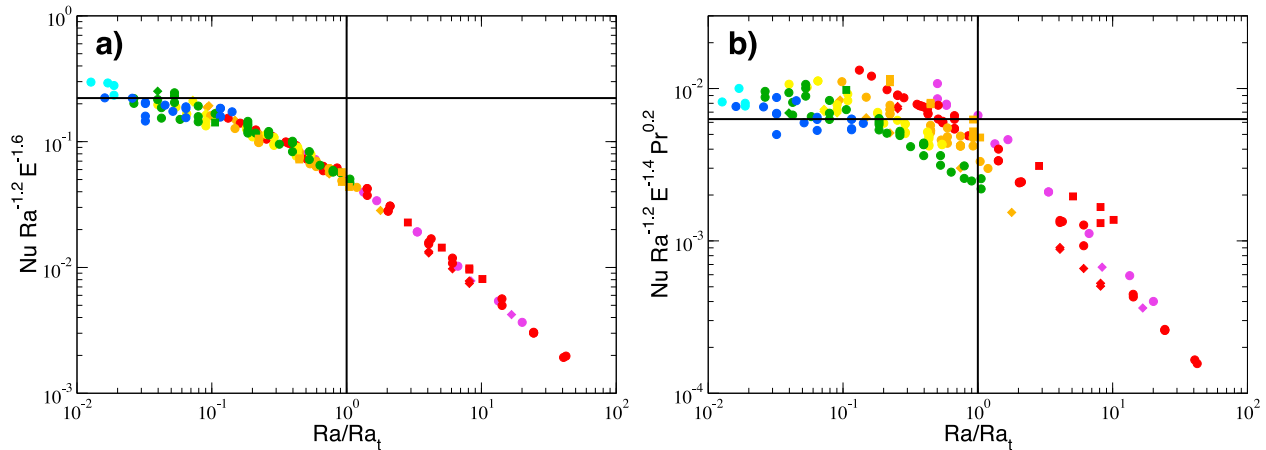
Figure 7. Goodness of fit tests for two rapidly rotating heat transfer scaling laws. Heat transfer data (Nu) normalized by each scaling law are plotted versus the boundary layer transition parameter, Ra/Ra_t. Symbols are the same as in Figure 4. (a) The Nusselt number normalized by the rapidly rotating scaling law (6). The horizontal line represents the rapidly rotating scaling law, $Nu = (Ra/Ra_c)^{6/5}$ with $Ra_c = 3.5E^{-4/3}$. (b) The Nusselt number normalized by the diffusivity free scaling (18). The horizontal line represents the diffusivity free scaling, $Nu^* = 0.1Ra_Q^{*6/11}$.

broader range of Rayleigh numbers within this regime, lower Ekman number simulations must be carried out. Until a clear asymptotic regime of highly supercritical ($Ra/Ra_c \gg 1$), rapidly rotating ($Ra/Ra_t < 1$) convection is reached, the veracity of any such scaling law is questionable.

[33] The diffusivity-free heat transfer scaling (18) is one member of a suite of empirical, diffusivity-free scaling laws. Within the range of parameter space currently accessible, this rotationally dependent diffusivity-free approach has produced scalings for several other model outputs such as typical velocities, length scales, and magnetic field strengths [*Christensen*, 2002; *Aubert*, 2005; *Olson and Christensen*, 2006; *Christensen et al.*, 2009]. These scaling laws implicitly take the rotation period as their dominant time scale, replacing the typical diffusion time scales present in the base parameters (Table 1). We have demonstrated here that heat transfer behavior is no longer controlled by rotation rate when $Ra \gtrsim Ra_t$ (Figures 5 and 7). Therefore, we postulate that Ra_t provides an upper bound for the application of the other diffusivity-free scaling laws of *Aubert* [2005], *Christensen and Aubert* [2006], *Olson and Christensen* [2006], and *Christensen et al.* [2009].

5. Mean Temperature Profiles and Thermal Mixing

[34] The rapidly rotating and weakly rotating heat transfer regimes exhibit different global thermal signatures. Figures 8 and 9 illustrate the transition in the mean temperature structures between the regimes. The rapidly rotating regime maintains large-scale mean internal temperature gradients while the weakly rotating regime undergoes vigorous mixing that produces an adiabatic interior fluid. (Mixing is a scale-dependent concept; here we consider mixing on the largest length scales of the system.) Since we consider Boussinesq convection, an adiabatic profile corresponds to a statistically isothermal interior fluid. This isothermalization of bulk fluid by convection has been observed in nonrotating [*Belmonte et al.*, 1994; *Camussi and Verzicco*, 1998] and weakly rotating convection [*Aurnou et al.*, 2007; *King et al.*, 2009], and is typically associated with chaotic, three dimensional turbulence. In rapidly rotating convection, however, the persistence of coherent thermal structures limits mixing, thereby permitting the establishment of significant nonzero mean temperature gradients within the bulk fluid [e.g., *Julien et al.*, 1996; *Gillet and Jones*, 2006; *Sprague et al.*, 2006; *King et al.*, 2009]. Figure 8 also shows that mean, meridional temperature structures exist in the rapidly rotating regime. This implies that the influence of rotation may promote large-scale baroclinicity in convection [cf. *Kaspi et al.*, 2009; *Jones and Kuzanyan*, 2009].

[35] We quantify the internal temperature gradients through calculations of the mean temperature lapse rate (i.e., the radial gradient of the temporally averaged temperature field, $d\bar{T}/dr$) at midshell for each of the dynamo subset models. A perfectly well mixed Boussinesq fluid will have a zero mean
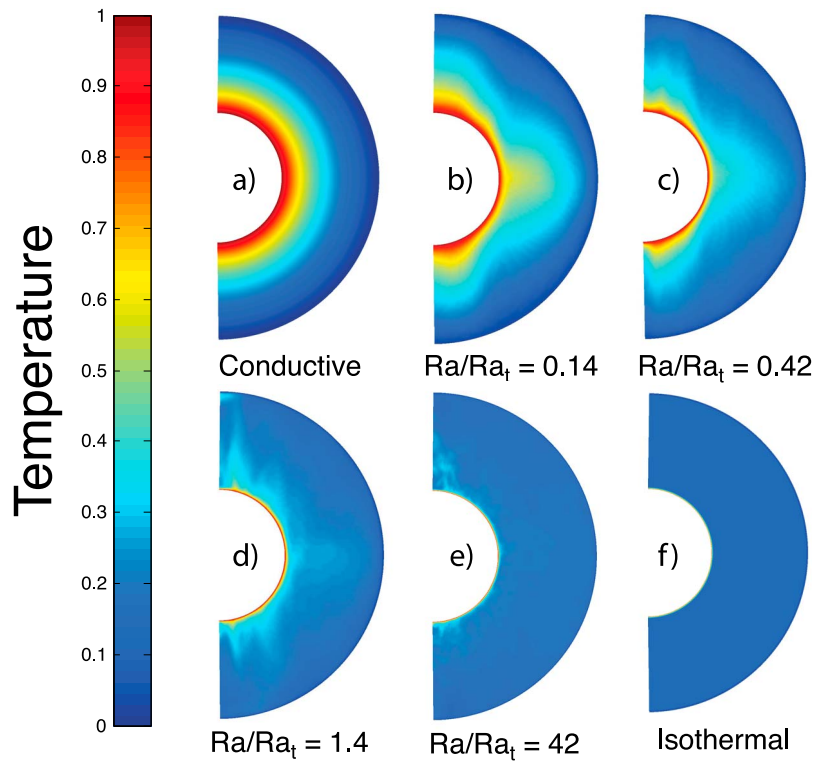
Figure 8. Meridional slices of time-averaged temperatures $((T - T_o)/\Delta T)$ from the dynamo subset. (a) Conductive end-member case for convective mixing, from (20). Cases (b) A, (c) B, (d) C, and (e) D in Table 2. Figures 8b and 8c show cases in the rapidly rotating regime ($Ra < Ra_t$); Figures 8d and 8e show cases in the weakly rotating regime ($Ra > Ra_t$). (f) Isothermal end-member case for convective mixing, from (28).
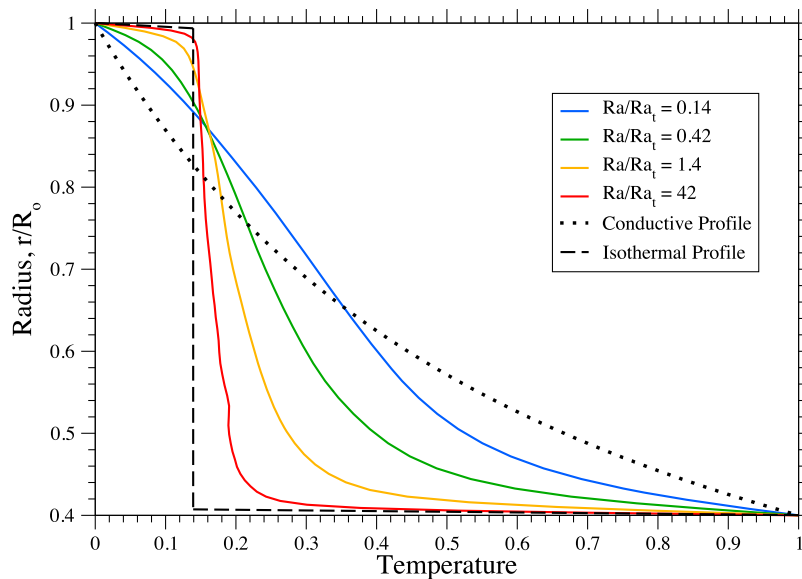

Figure 9. Mean radial temperature profiles from the dynamo subset cases shown in Figure 8. Temperature is normalized as $(T - T_o)/\Delta T$, and radial position is normalized by the outer boundary radius. The dotted line indicates the conductive temperature profile from (20), and the dashed line represents the idealized isothermal temperature profile, $T = T_o + 0.14\Delta T$, from (28) with $\chi = 0.4$. Note that the internal temperature gradients approach zero as Ra/Ra_t increases.
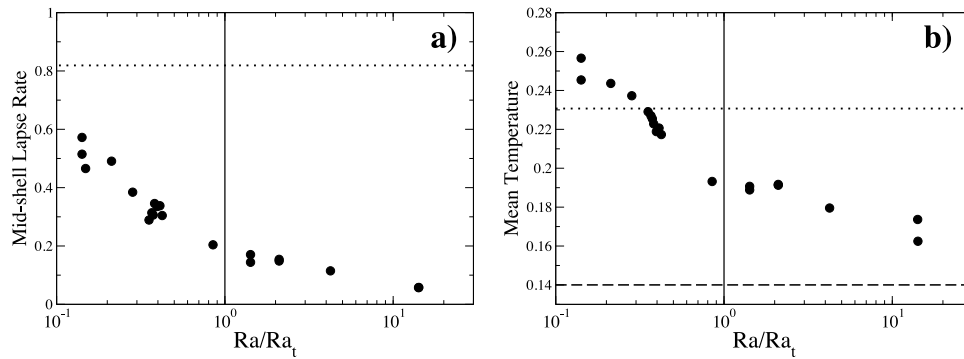
Figure 10. (a) Nondimensional temperature lapse rate, $|\frac{dT}{dr}\frac{R_o-R_i}{\Delta T}|$, at midshell ($r = (R_i + R_o)/2$) versus the boundary layer transition parameter, Ra/Ra_t, for the dynamo subset. The dotted line represents the conductive lapse rate at midshell (using (20) and $\chi = 0.4$): $\frac{dT}{dr} = -\Delta T \frac{R_o R_i}{R_o-R_i}r^{-2} = -0.82\frac{\Delta T}{R_o-R_i}$. (b) Mean internal temperature, $(\langle T \rangle - T_o)/\Delta T$, versus the boundary layer transition parameter, Ra/Ra_t, from the dynamo subset models. The dotted line indicates the mean temperature of a conductive shell, $\langle T \rangle = T_o + 0.23\Delta T$, from (21) with $\chi = 0.4$. The dashed line represents a mean temperature estimate for well-mixed convection, $\langle T \rangle = T_o + 0.14\Delta T$, from (28) with $\chi = 0.4$.

temperature gradient in the interior fluid, $d\overline{T}/dr = 0$, such that the bulk fluid is isothermal. As the influence of rotation grows (for decreasing Ra/Ra_t), some rigidity is imparted on the flow via the Coriolis force, and increasingly strong thermal gradients can abide, as shown by *King et al.* [2009].

[36] Figure 10a shows measurements of midshell lapse rates from the dynamo subset. We observe a transformation from a nearly conductive thermal signature in the rotationally controlled regime ($Ra < Ra_t$) to a nearly isothermal interior fluid in the weakly rotating regime ($Ra > Ra_t$). The transition to the nonrotating heat transfer scaling, $Nu \sim Ra^{2/7}$, is therefore linked to the elimination of mean interior temperature gradients by efficient convective mixing. In the rapidly rotating heat transfer regime, however, the persistence of mean temperature gradients indicates that strong thermal mixing is inhibited by the influence of rotation.

[37] The lapse rate behavior in Figure 10a illustrates the relationship between heat transfer regimes and thermal mixing in a limited subset of our dynamo model data. In order to investigate mixing more systematically, we would like to quantify the strength of mean thermal gradients in the broader array of dynamo factory models. However, we do not have lapse rate data for these models. Instead, we use volume-averaged temperature calculations as a proximate measure of internal temperature gradients.

[38] Figure 10b shows mean internal temperatures from the dynamo subset models. The mean internal temperature is the average temperature over the volume of the shell, $(\langle T \rangle - T_o)/\Delta T$, where $\langle \cdot \rangle$

indicates volume averaging. A comparison of Figures 10a and 10b shows that the lapse rates and mean internal temperatures display qualitatively similar behavior. In the following paragraphs, we relate mean temperature to the efficiency of thermal mixing by comparing model data against the two idealized end-member cases: a conductive and an isothermal temperature profile.

[39] First, in an incompressible spherical shell with isothermal boundaries, the conductive case will have a temperature profile of the form [*Kono and Roberts*, 2001]:

$$T(r) = T_o + \left(\frac{R_o R_i}{R_o - R_i}\left(\frac{1}{r} - \frac{1}{R_o}\right)\right)\Delta T, \quad (20)$$

where R_o and R_i are the radii of the outer and inner boundaries, respectively, and T_o and $T_o + \Delta T$ are the imposed outer and inner boundary temperatures, respectively. This expression can also be written in terms of the shell's radius ratio, $\chi = R_o/R_i$ as

$$T(r) = T_o + \left(\frac{\chi}{\chi - 1}\left[1 - (r/R_o)^{-1}\right]\right)\Delta T, \quad (21)$$

We can integrate (20) over the volume of the shell to solve for the mean temperature for a conductive fluid:

$$\langle T_{\text{conductive}} \rangle = T_o + \left(\frac{R_o + 2R_i}{R_o^2 + R_o R_i + R_i^2}\right)\frac{\Delta T}{2}. \quad (22)$$

This expression can also be written in terms of the shell's radius ratio as

$$\langle T_{\text{conductive}} \rangle = T_o + \left(\frac{\chi(1 + 2\chi)}{1 + \chi + \chi^2}\right)\frac{\Delta T}{2}. \quad (23)$$
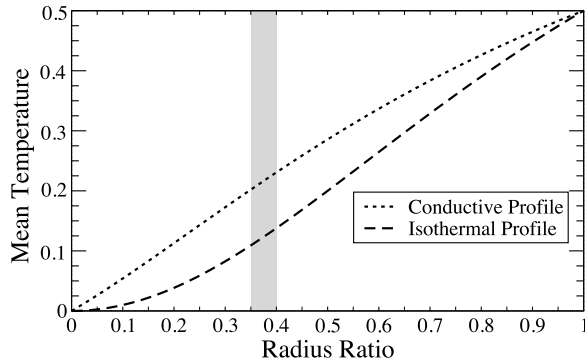
Figure 11. Theoretical mean shell temperature versus the radius ratio, $\chi = R_i/R_o$. The mean temperature is the average temperature over the volume of the shell, $(\langle T \rangle - T_o)/\Delta T$. The dotted and dashed lines represent predicted mean temperature from (23) and (28), respectively. The gray region indicates that occupied by the present dynamo models.

With the dynamo factory model's radius ratio of $\chi = 0.35$, we then predict an average temperature of

$$\langle T_{\text{conductive}} \rangle = T_o + 0.21\Delta T \qquad (24)$$

for the conductive case.

[40] Second, we can estimate the mean temperature from a well-mixed temperature profile. In this configuration, we assume the fluid is composed of two regions: the boundary layers (inner and outer), and the interior fluid, also called the bulk fluid. The interior fluid is isothermal and makes up the vast majority of the fluid by volume. We also assume that inner and outer thermal boundary layers have equal thickness, which we qualitatively observe to hold true in dynamo subset temperature profiles. The temperature drop across the inner and outer thermal boundary layers is δT_i and δT_o, respectively. Conservation of outward heat flux through concentric spherical surfaces dictates that

$$\frac{\delta T_i}{\delta T_o} = \left(\frac{R_o}{R_i}\right)^2 = \chi^{-2}. \qquad (25)$$

An isothermal interior further implies the entirety of the temperature drop occurs in the thin boundary layers:

$$\delta T_i + \delta T_o = \Delta T; \qquad (26)$$

and the interior temperature will be that at the bulk edge of the thermal boundary layers:

$$T_{\text{interior}} = T_o + \delta T_o = (T_o + \Delta T) - \delta T_i. \qquad (27)$$

Manipulating equations (25)–(27) then gives temperature of the interior fluid to be:

$$T_{\text{interior}} = T_o + \left(1 + \chi^{-2}\right)^{-1}\Delta T. \qquad (28)$$

Thus, shell aspect ratio of $\chi = R_i/R_o = 0.35$ gives an interior fluid temperature of

$$T_{\text{interior}} = T_o + 0.11\Delta T. \qquad (29)$$

If we ignore the contribution to the mean temperature by that within the thin boundary layers, the mean shell temperature for this end case is the temperature to which the interior isothermalizes:

$$\langle T_{\text{isothermal}} \rangle = T_{\text{interior}}. \qquad (30)$$

[41] Figure 11 illustrates how each of these two end member predictions varies with the radius ratio, χ. The dotted line represents the mean conductive temperature from (23); and the dashed line represents the mean isothermal temperature from (28). The dynamo models have $\chi = 0.35$ and $\chi = 0.4$, which is indicated by the gray region.

[42] Figure 12a shows mean internal temperature calculations from the dynamo factory models in comparison with the end case predictions. Models with $Ra < Ra_t$ approach conductive (dotted line) mean temperatures, which indicates the persistence of strong, large-scale thermal gradients in the bulk fluid. The lowest Ra/Ra_t cases have warmer than conductive mean temperatures. This is likely due to the warming of the outer region of the shell, where the bulk of the fluid volume resides, relative to a conductive profile near the onset of convection (see $Ra/Ra_t = 0.14$ case in Figure 9). When $Ra > Ra_t$, the thermal signature appears to asymptotically approach the well-mixed, adiabatic end member (dashed line). This illustrates the increasing efficiency of thermal mixing as the influence of rotation is diminished in planetary dynamo models. Furthermore, the collapse of mean temperature data by the boundary layer transition parameter, Ra/Ra_t, indicates that boundary layer processes are directly related to the interior temperature field.

[43] Convective regions in planets and stars are typically assumed to be well mixed on account of their strongly turbulent nature. The Reynolds number, Re, compares inertial and viscous forces on global length scales, and is thought of as a parameterization of the degree of turbulence (see Table 1 for definition). High Re fluids in the absence of rotation are dispersive media wherein
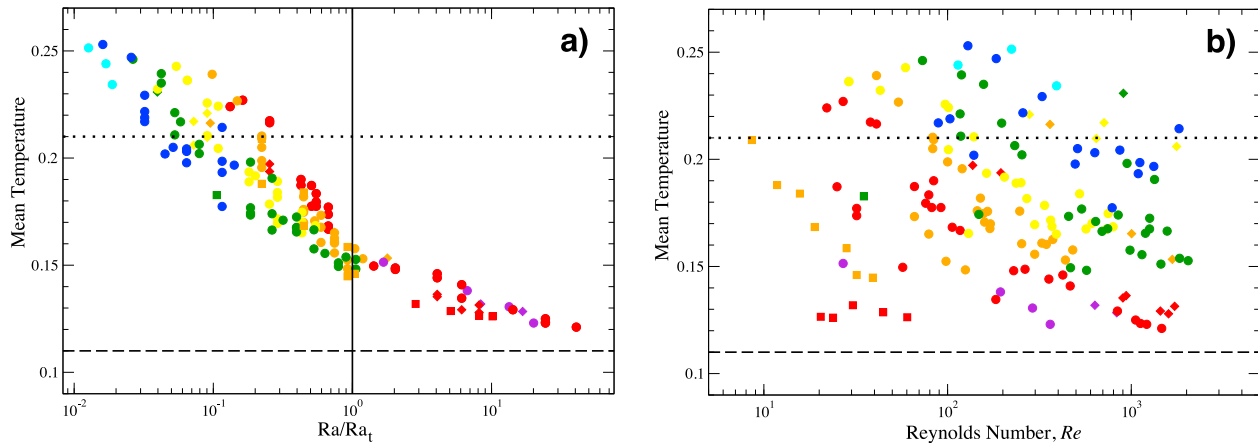
Figure 12. Mean internal temperature, $(\langle T \rangle - T_o)/\Delta T$, from the dynamo factory data set. (a) Mean temperature plotted versus the boundary layer transition parameter, Ra/Ra_t. (b) Mean temperature plotted versus the Reynolds number, Re. Symbols are the same as in Figure 4. Mean temperatures near the conductive estimate (dotted line, $T = T_o + 0.21\Delta T$) are considered poorly mixed. Those near the isothermal estimate (dashed line, $T = T_o + 0.11\Delta T$) are considered well mixed.

gradients of passive scalars are quickly smoothed [*McWilliams*, 2006]. We may expect, then, that the thermal mixing observed in the dynamo models may be strongly influenced by Re.

[44] Figure 12b shows the mean temperature measurements as in Figure 12a, but now plotted against the Reynolds number. We observe no dependence of thermal mixing on Re. Instead, a comparison of Figures 12a and 12b shows that Ra/Ra_t, not the Reynolds number, characterizes thermal mixing in dynamo models.

6. Application to Earth's Core

6.1. Convective Regime of the Core

[45] Assuming the empirical scaling laws derived here apply to Earth's core, we can estimate the Rayleigh number and heat transfer regime of the core. Estimates of the total superadiabatic heat flux escaping the core mantle boundary (CMB) typically fall in the range 1–10 TW [e.g., *Buffett*, 2003]. We can use these heat flux estimates, along with estimates of the thermophysical properties of core fluid, to determine the flux Rayleigh number in the core. The flux Rayleigh number is defined as

$$Rf = Ra\, Nu = \frac{\alpha_T\, g\, Q\, L^4}{A\, \rho\, c_P\, \nu\, \kappa^2}, \tag{31}$$

where Q is the total superadiabatic heat flux, A is the surface area of the CMB, and c_P is the specific

heat of the core fluid. The flux Rayleigh number has the advantage of depending on Q, rather than the superadiabatic temperature drop across the core, ΔT, which is less well constrained from geophysical observations.

[46] Estimates of core properties are listed in Table 3. Given these properties, the flux Rayleigh number is estimated to lie in the range

$$Rf \approx (2.4 - 24) \times 10^{28} \tag{32}$$

Table 3. Estimates of the Physical Properties of Earth's Core[a]

Property	Core Estimate	Reference
α_T	10^{-5} K^{-1}	*Gubbins* [2001]
g	10 m/s^2	*Dziewonski and Anderson* [1981]
Q	$(1{-}10) \times 10^{12}$ W	*Buffett* [2003]
L	2260 km	*Dziewonski and Anderson* [1981]
A	1.5×10^{14} m^2	*Dziewonski and Anderson* [1981]
ρ	10^4 kg/m^3	*Dziewonski and Anderson* [1981]
c_P	700 J/kgK	*Gubbins* [2001]
ν	10^{-6} m^2/s	*de Wijs et al.* [1998]
κ	10^{-5} m^2/s	*Gubbins* [2001]
Ω	7.3×10^{-5} rad/s	*McCarthy and Babcock* [1986]

[a]Properties are as follows: α_T is the fluid's coefficient of thermal expansivity, g is gravitational acceleration, Q is total superadiabatic heat flux, L is the distance between inner core boundary (ICB) and core-mantle boundary (CMB), A is the surface area of the CMB, ρ is the density of the fluid, c_P is the fluid's specific heat, ν is the kinematic viscosity of the fluid, κ is the fluid's thermal diffusivity, and Ω is the angular rotation rate.

in Earth's core. We can also use these core property estimates to determine an Ekman number for the core:

$$E \approx 1.3 \times 10^{-15}. \tag{33}$$

[47] The heat transfer regime of the core is determined by comparing the estimated core Rf value with a transitional flux Rayleigh number, which can be written as

$$Rf_t \approx Ra_t Nu_t \sim E^{-9/4}, \tag{34}$$

and has an approximate value of $Rf_t \approx 2 \times 10^{32}$ in the core. The appropriate heat transfer scaling law for $Rf < Rf_t$ is $Nu \approx (Ra/Ra_c)^{6/5}$, which, together with our estimate of Rf, allows us to solve for the range of Rayleigh and Nusselt numbers for core convection:

$$Ra \approx (1-3) \times 10^{24} \quad ; \quad Nu \approx (2-8) \times 10^4. \tag{35}$$

Note that these values correspond to the diabatic component of core thermodynamics. For example, heat conducted down the core adiabat is estimated to be on the same order as that transported by convection, giving a different formulation of the Nusselt number, a total Nusselt number, of approximately 2 [e.g., *Buffett*, 2003].

[48] Using the estimate for E given above, the transitional Rayleigh number in the core is $Ra_t = E^{-7/4} \approx 10^{26}$. We then estimate that Ra/Ra_t in the core is roughly in the range:

$$Ra/Ra_t \approx (1-3) \times 10^{-2}. \tag{36}$$

Thus, our results suggest that core convection occurs in the rapidly rotating regime, but only just barely.

[49] As mentioned in section 2.1, previous work has sought to separate these two regimes based on measurements of the vigor of convective flow in various models [*Olson and Christensen*, 2006; *Schmitz and Tilgner*, 2009]. *Olson and Christensen* [2006] extrapolate scalings of local Rossby numbers in planetary dynamo models to predict that Earth's core falls just before the transition from rotationally dominated magnetic field morphology to that nearly unaffected by rotation. *Schmitz and Tilgner* [2009] extrapolate calculations of a modified Peclet number from rotating convection simulations to Earth's core using estimates of convective speeds from geomagnetic secular variation inversions. The authors predict that core convection lies within a transitional region between rapidly rotating and weakly rotating regimes. Thus,

though by different means, the present work and these previous studies all place core convection near, but below, the nonrotating style convective regime.

[50] We speculate that Earth's proximity to the transition is important for dynamics such as magnetic field morphology and polarity reversals. In particular, the rough alignment of Earth's dominant dipole and rotation axis suggests that core flow is strongly influenced by rotation. However, the indirect observation of geomagnetic polarity reversals from seafloor striping hints at strong nonlinearities typical of more chaotic fluid dynamics. Our estimate that core convection resides in the rapidly rotating regime, but near the transition to weakly rotating behavior, provides a possible explanation of this dichotomy. Studies of polarity reversals in dynamo models find that the generation of predominantly dipolar, reversing magnetic fields typically occurs in a relatively narrow range of parameters between rotationally dominated and buoyancy dominated dynamo regimes [e.g., *Wicht et al.*, 2009; *Driscoll and Olson*, 2009].

[51] Convection in Earth's core is likely driven by some combination of thermal and compositional buoyancy [e.g., *Braginsky and Roberts*, 1995]. Compositional convection may arise as lighter, alloy rich liquid metal is formed near the bottom of the core from the solidification of the inner core. Similarly, chemical reactions at the core mantle boundary may generate compositionally heavy fluid. The chemical diffusivities of these fluid mixtures may be lower than that expected of thermal diffusivity in the core by about three orders of magnitude [e.g., *Gubbins*, 2001]. This would result in larger estimates of the effective core Prandtl number and Rayleigh number (and therefore Ra/Ra_t). The simulations presented here consider only thermal convection. It is unclear how the inclusion of compositional convection dynamics would alter our results [cf. *Kutzner and Christensen*, 2000], especially in regard to the arguments derived from boundary layer physics.

6.2. Convective Mixing in the Core

[52] We can also apply the analysis of thermal mixing in dynamo models (section 5) to Earth's core. It is typically assumed that the strong turbulence in the core, where $Re \sim 10^8$ [*Bloxham and Jackson*, 1991], effectively mixes the bulk core fluid [e.g., *Stacey*, 1969; *Stevenson*, 1987; *Braginsky and Roberts*, 1995; *Jones*, 2009]. Here we show that thermal mixing is not strongly dependent on the

Table 4. A Summary of Heat Transfer Results[a]

	Rapidly Rotating Regime	Weakly Rotating Regime
Criterion	$Ra \lesssim Ra_t = E^{-7/4}$	$Ra \gtrsim Ra_t = E^{-7/4}$
Heat transfer scaling	$Nu \approx (Ra/Ra_c)^{6/5}$	$Nu \approx C\, Ra^{2/7}$
Planar scaling constant	$Ra_c = 6E^{-4/3}$	$C = 0.16$
Spherical scaling constant	$Ra_c = 3.5E^{-4/3}$	$C = 0.075$

[a]Scaling constants from the present analysis of spherical dynamo models are compared with those from the plane layer, nonmagnetic rotating convection study of *King et al.* [2009].

degree of turbulence as characterized by the Reynolds number. Instead, the efficiency of mixing by convection is linked to the relative importance of rotation. We estimate that Earth's core lies in the rapidly rotating regime, since $Ra < Ra_t$. Through measurements of the mean temperature of dynamo models, we have shown that significant superadiabatic density gradients persist in the rapidly rotating regime, independent of the vigor of flow, Re. This implies that large-scale superadiabatic density anomalies may survive in the core, which would not be permitted by considerations of turbulent mixing without rotation. That is, rapidly rotating convection systems, like Earth's core, may not be strictly adiabatic.

[53] Interestingly, deviations from expected density profiles have been inferred seismically in the core [e.g., *Romanowicz and Breger*, 2000; *Soldati et al.*, 2003]. Notable features include thick (~300–400 km) regions of anomalous seismic wave velocities at the top [*Souriau and Poupinet*, 1991] and bottom [*Kaneshima et al.*, 1994] of the core. Furthermore, recent seismic studies have shown that observationally significant temporal fluctuations in density occur in Earth's outer core [*Dai and Song*, 2008]. It has been argued that such observations may be due to perturbations of geopotential surfaces in the core by density heterogeneity in the mantle [*Wahr and de Vries*, 1989]. However, it does not appear that this argument can explain the decadal time scale variations observed by *Dai and Song* [2008].

[54] We can estimate the total superadiabatic density drop across the core using our estimate of the Rayleigh number (35) and the thermophysical properties listed in Table 3. The superadiabatic temperature drop across the outer core is then $\Delta T \approx 10^{-2}$ K, giving a total superadiabatic density change

of $\Delta \rho / \rho_o \approx \alpha_T \Delta T \approx 10^{-7}$. This estimate represents a rough upper bound for mean density anomalies that may persist in the bulk of the outer core, and cannot account for the amplitude of density variations inferred from several of the seismic studies, which may be as large as $\Delta \rho / \rho_o \approx 10^{-3}$ [*Soldati et al.*, 2003; *Dai and Song*, 2008].

7. Summary

[55] We hypothesize that heat transfer results found in the nonmagnetic, plane layer convection study of *King et al.* [2009] also applies to planetary dynamo models. This hypothesis predicts that heat transfer occurs in two separate regimes, rapidly rotating and weakly rotating, with empirical heat transfer scalings in each regime, $Nu \sim (Ra/Ra_c)^{6/5}$ and $Nu \sim Ra^{2/7}$, respectively. Second, the transition between regimes is determined by relative thicknesses of the thermal and velocity boundary layers, and is described by the transitional Rayleigh number, $Ra_t = E^{-7/4}$.

[56] We test this hypothesis using a broad array of numerical planetary dynamo models, and our heat transfer scaling results are summarized in Table 4. Heat transfer behavior in the dynamo models does exist in two distinct regimes, which are adequately separated by the transitional Rayleigh number (Figure 5). In the rapidly rotating regime ($Ra \lesssim Ra_t$), heat transfer is described by the scaling $Nu = (Ra/Ra_c)^{6/5}$, where $Ra_c = 3.5E^{-4/3}$. In the weakly rotating regime ($Ra \gtrsim Ra_t$), heat transfer follows a $Nu = 0.075 Ra^{2/7}$ scaling. The $Nu \sim Ra^{2/7}$ scaling implies that heat transfer in weakly rotating spherical systems is similar to that in nonrotating planar convection. In the rapidly rotating regime, Nu is significantly less than that expected for nonrotating convection because the influence of rotation inhibits convective heat transfer. Interestingly, our collapse of the heat transfer behavior is not explicitly dependent on magnetic field strength of these dynamo models.

[57] Based on the boundary layer thickness calculations shown in Figure 6, we argue that the transition between these regimes is governed by the relative thicknesses of the thermal and velocity boundary layers. Thus, despite numerous differences between the convection system examined by *King et al.* [2009] and the dynamo models analyzed in this work, the basic heat transfer behavior of the two studies is in agreement.

[58] Models in each of the two heat transfer regimes produce different thermal profiles. The rapidly rotating regime is distinguished by signifi-

cant, large-scale thermal gradients. Therefore, the strong influence of rotation on core convection may imply that seismically observable density structures can exist. In contrast, models residing in the weakly rotating regime are well mixed, producing nearly isothermal interiors. Thermal mixing is shown to depend on the boundary layer controlled transition parameter, Ra/Ra_t (Figure 12a), and is not observed to depend on the Reynolds number (Figure 12b). Our results appear to imply that rotational effects on convective mixing may provide a dynamical mechanism for the seismically inferred density heterogeneities in the outer core [e.g., *Romanowicz and Breger*, 2000; *Soldati et al.*, 2003]. However, when extrapolated to core conditions, our heat transfer scalings predict a Rayleigh number of $Ra \approx 2 \times 10^{24}$ in the core, corresponding to a super-adiabatic density variation of $\Delta\rho/\rho_o \approx 10^{-7}$, which cannot explain the seismically inferred anomalies.

Acknowledgments

References

Aubert, J. (2005), Steady zonal flows in spherical shell dynamos, *J. Fluid Mech.*, *542*, 53–67.

Aurnou, J. (2007), Planetary core dynamics and convective heat transfer scaling, *Geophys. Astrophys. Fluid Dyn.*, *101*(5–6), 327–345.

Aurnou, J., and P. Olson (2001), Experiments on Rayleigh-Bénard convection, magnetoconvection and rotating magnetoconvection in liquid gallium, *J. Fluid Mech.*, *430*, 283–307.

Aurnou, J., M. Heimpel, and J. Wicht (2007), The effects of vigorous mixing in a convective model of zonal flow on the ice giants, *Icarus*, *190*, 110–126.

Aurnou, J., M. Heimpel, L. Allen, E. King, and J. Wicht (2008), Convective heat transfer and the pattern of thermal emission on the gas giants, *Geophys. J. Int.*, *173*(3), 793–801.

Belmonte, A., A. Tilgner, and A. Libchaber (1994), Temperature and velocity boundary layers in turbulent convection, *Phys. Rev. E*, *50*(1), 269–280.

Bloxham, J., and A. Jackson (1991), Fluid flow near the surface of Earth's outer core, *Rev. Geophys.*, *29*(1), 97–120.

Boubnov, B., and G. Golitsyn (1990), Temperature and velocity-field regimes of convective motions in a rotating plane fluid layer, *J. Fluid Mech.*, *219*, 215–239.

Braginsky, S., and P. Roberts (1995), Equations governing convection in Earth's core and the geodynamo, *Geophys. Astrophys. Fluid Dyn.*, *79*, 1–97.

Buffett, B. (2003), The thermal state of Earth's core, *Science*, *299*(5613), 1675–1677.

Busse, F. (1970), Thermal instabilities in rapidly rotating systems, *J. Fluid Mech.*, *44*(3), 441–460.

Camussi, R., and R. Verzicco (1998), Convective turbulence in mercury: Scaling laws and spectra, *Phys. Fluids*, *10*(2), 516–527.

Canuto, V., and M. Dubovikov (1998), Two scaling regimes for rotating Rayleigh-Bénard convection, *Phys. Rev. Lett.*, *80*(2), 281–284.

Castaing, B., G. Gunaratne, F. Heslot, L. Kadanoff, A. Libchaber, S. Thomae, X. Wu, S. Zaleski, and G. Zanetti (1989), Scaling of hard turbulence in Rayleigh-Bénard convection, *J. Fluid Mech.*, *204*, 1–30.

Chandrasekhar, S. (1953), The instability of a layer of fluid heated below and subject to Coriolis forces, *Proc. R. Soc. London, Ser. A*, *217*(1130), 306–327.

Chandrasekhar, S. (1954), The instability of a layer of fluid heated below and subject to the simultaneous sction of a magnetic field and rotation, *Proc. R. Soc. London, Ser. A*, *225*(1161), 173–184.

Christensen, U. (2002), Zonal flow driven by strongly supercritical convection in rotating spherical shells, *J. Fluid Mech.*, *470*, 115–133.

Christensen, U., and J. Aubert (2006), Scaling properties of convection-driven dynamos in rotating spherical shells and application to planetary magnetic fields, *Geophys. J. Int.*, *166*(1), 97–114.

Christensen, U., P. Olson, and G. Glatzmaier (1999), Numerical modelling of the geodynamo: A systematic parameter study, *Geophys. J. Int.*, *138*(2), 393–409.

Christensen, U., V. Holzwarth, and A. Reiners (2009), Energy flux determines magnetic field strength of planets and stars, *Nature*, *457*(7226), 167–169.

Cioni, S., S. Chaumat, and J. Sommeria (2000), Effect of a vertical magnetic field on turbulent Rayleigh-Bénard convection, *Phys. Rev. E*, *62*(4), 4520–4523.

Dai, W., and X. Song (2008), Detection of motion and heterogeneity in Earth's liquid outer core, *Geophys. Res. Lett.*, *35*, L16311, doi:10.1029/2008GL034895.

Debnath, L. (1973), On Ekman and Hartmann boundary layers in a rotating fluid, *Acta Mech.*, *18*, 333–341.

Desjardins, B., E. Dormy, and E. Grenier (2001), Instability of Ekman-Hartmann boundary layers, with application to the fluid flow near the core-mantle boundary, *Phys. Earth Planet. Inter.*, *124*, 283–294.

de Wijs, G., G. Kresse, L. Vocadlo, D. Dobson, D. Alfe, M. J. Fillan, and G. D. Price (1998), The viscosity of liquid iron at the physical conditions of the Earth's core, *Nature*, *392*, 805–807.

Dormy, E., A. Soward, C. Jones, and D. Jault (2004), The onset of thermal convection in rotating spherical shells, *J. Fluid Mech.*, *501*, 43–70.

Driscoll, P., and P. Olson (2009), Effects of buoyancy and rotation on the polarity reversal frequency of gravitationally driven numerical dynamos, *Geophys. J. Int.*, *178*(3), 1337–1350.

Dziewonski, A., and D. Anderson (1981), Preliminary reference Earth model, *Phys. Earth Planet. Inter.*, *25*, 297–356.

Eltayeb, I., and P. Roberts (1970), Hydromagnetics of rotating fluids, *Astrophys. J.*, *162*(2), 699–701.

Fearn, D. (1998), Hydromagnetic flow in planetary cores, *Rep. Prog. Phys.*, *61*, 175–235.

Gillet, N., and C. Jones (2006), The quasi-geostrophic model for rapidly rotating spherical convection outside the tangent cylinder, *J. Fluid Mech.*, *554*, 343–369.

Gilman, P. (1977), Nonlinear dynamics of boussinesq convection in a deep rotating spherical shell-i, *Geophys. Astrophys. Fluid Dyn.*, *8*(1), 93–135.

Gilman, P., and E. Benton (1968), Influence of an axial magnetic field on the steady linear Ekman boundary layer, *Phys. Fluids*, *11*(11), 2397–2401.

Glatzmaier, G. (1984), Numerical simulations of stellar convective dynamos. I. The model and method, *J. Comput. Phys.*, *55*(3), 461–484.

Glazier, J., T. Segawa, A. Naert, and M. Sano (1999), Evidence against 'ultrahard' thermal turbulence at very high Rayleigh numbers, *Nature*, *398*, 307–310.

Greenspan, H. (1968), *The Theory of Rotating Fluids*, Cambridge Univ. Press, London.

Gubbins, D. (2001), The Rayleigh number for convection in the Earth's core, *Phys. Earth Planet. Inter.*, *128*, 3–12.

Gubbins, D., and P. Roberts (1987), Magnetohydrodynamics of the Earth's core, in *Geomagnetism*, edited by J. A. Jacobs, pp. 1–183, Academic, London.

Heimpel, M., J. Aurnou, and J. Wicht (2005), Simulation of equatorial and high-latitude jets on Jupiter in a deep convection model, *Nature*, *438*(7065), 193–196.

Jones, C. A. (2009), Thermal and compositional convection in the outer core, in *Treatise on Geophysics*, vol. 8, *Core Dynamics*, pp. 131–185, Elsevier, Amsterdam.

Jones, C., and K. Kuzanyan (2009), Compressible convection in the deep atmospheres of giant planets, *Icarus*, *204*, 227–238.

Jones, C., A. Soward, and A. Mussa (2000), The onset of thermal convection in a rapidly rotating sphere, *J. Fluid Mech.*, *405*, 157–179.

Julien, K., S. Legg, J. McWilliams, and J. Werne (1996), Rapidly rotating turbulent Rayleigh-Bénard convection, *J. Fluid Mech.*, *322*, 243–273.

Kaneshima, S., K. Hirahara, and T. Ohtaki (1994), Seismic structure near the inner core-outer core boundary, *Geophys. Res. Lett.*, *21*(2), 157–160.

Käpylä, P. J., M. J. Korpi, and A. Brandenburg (2009), Large-scale dynamos in rigidly rotating turblent convection, *Astrophys. J.*, *697*(2), 1153–1163.

Kaspi, Y., G. Flierl, and A. Showman (2009), The deep wind structure of the giant planets: Results from an anelastic general circulation model, *Icarus*, *202*, 525–542.

King, E., S. Stellmach, J. Noir, U. Hansen, and J. Aurnou (2009), Boundary layer control of rotating convection systems, *Nature*, *457*(7227), 301–304.

Kolmogorov, A. (1941), The local structure of turbulence in incompressible viscous fluid for very large Reynolds numbers, *Dokl. Akad. Nauk SSSR*, *30*, 301–305.

Kono, M., and P. Roberts (2001), Definition of the Rayleigh number for geodynamo simulation, *Phys. Earth Planet. Inter.*, *128*, 13–24.

Kutzner, C., and U. Christensen (2000), Effects of driving mechanisms in geodynamo models, *Geophys. Res. Lett.*, *27*(1), 29–32.

Kutzner, C., and U. Christensen (2002), From stable dipolar towards reversing numerical dynamos, *Phys. Earth Planet. Inter.*, *131*, 29–45.

Liu, Y., and R. Ecke (2009), Heat transport measurements in turbulent rotating rayleigh-benard convection, *Phys. Rev. E*, *80*(3), 6314–6325.

McCarthy, D., and A. Babcock (1986), The length of day since 1656, *Phys. Earth Planet. Inter.*, *44*, 281–292.

McWilliams, J. (2006), *Fundamentals of Geophysical Fluid Dynamics*, Cambridge Univ. Press, Cambridge, U. K.

Miesch, M. (2005), Large-scale dynamics of the convection zone and tachocline, *Living Rev. Sol. Phys.*, *2*, lrsp-2005-1.

Nakagawa, Y. (1959), Experiments on the instability of a layer of mercury heated from below and subject to the simultaneous action of a magnetic field and rotation, *Proc. R. Soc. London, Ser. A*, *249*(1256), 138–145.

Niemela, J., L. Skrbek, K. Sreenivasan, and R. Donnelly (2000), Turbulent convection at very high Rayleigh numbers, *Nature*, *404*, 837–840.

Olson, P., and U. Christensen (2006), Dipole moment scaling for convection-driven planetary dynamos, *Earth and Planetary Science Letters*, *250*, 561–571.

Palacios, A., A. Brun, and C. Saclay (2006), Simulation of turbulent convection in a slowly rotating red giant star, *Astron. Nachr.*, *999*(88), 789–793.

Roberts, P. (1968), On the thermal instability of a rotating fluid sphere containing heat sources, *Philos. Trans. R. Soc. London, Ser. A*, *263*(1136), 93–117.

Romanowicz, B., and L. Breger (2000), Anomalous splitting of free oscillations: A reevaluation of possible interpretations, *J. Geophys. Res.*, *105*(B9), 21,559–21,578.

Rossby, H. (1969), A study of Benard convection with and without rotation, *J. Fluid Mech.*, *36*(2), 309–335.

Schmitz, S., and A. Tilgner (2009), Heat transport in rotating convection without Ekman layers, *Phys. Rev. E*, *80*(1), 5305–5307.

Soldati, G., L. Boschi, and A. Piersanti (2003), Outer core density heterogeneity and the discrepancy between PKP and PcP travel time observations, *Geophys. Res. Lett.*, *30*(4), 1190, doi:10.1029/2002GL016647.

Souriau, A., and G. Poupinet (1991), A study of the outermost liquid core using differential travel times of the SKS, SKKS, and S3KS phases, *Phys. Earth Planet. Inter.*, *68*, 183–199.

Spiegel, E. (1971), Convection in stars. I. Basic Boussinesq convection, *Annu. Rev. Astron. Astrophys.*, *9*, 323–352.

Sprague, M., K. Julien, E. Knobloch, and J. Werne (2006), Numerical simulation of an asymptotically reduced system for rotationally constrained convection, *J. Fluid Mech.*, *551*, 141–174.

Stacey, F. (1969), *Physics of the Earth*, John Wiley, New York.

Stevenson, D. (1987), Limits on lateral density variations in the Earth's outer core, *Geophys. J. Int.*, *88*(1), 311–319.

Stevenson, D. (2003), Planetary magnetic fields, *Earth Planet. Sci. Lett.*, *208*, 1–11.

Tilgner, A. (1996), High-Rayleigh-number convection in spherical shells, *Phys. Rev. E*, *53*(5), 4847–4851.

Wahr, J., and D. de Vries (1989), The possibility of lateral structure inside the core and its implications for nutation and Earth tide observations, *Geophys. J. Int.*, *99*(3), 511–519, doi:10.1111/j.1365-246X.1989.tb02036.x.

Wicht, J. (2002), Inner-core conductivity in numerical dynamo simulations, *Phys. Earth Planet. Inter.*, *132*, 281–302.

Wicht, J., S. Stellmach, and H. Harder (2009), Numerical models of the geodynamo: From fundamental Cartesian models to 3D simulations of field reversals, in *Geomagnetic Field Variations*, edited by K. Glassmeier, H. Soffel, and J. Negendank, pp. 107–158, Springer, Berlin.

Zhang, K. (1995), Spherical shell rotating convection in the presence of a toroidal magnetic field, *Proc. R. Soc. London, Ser. A*, *448*(1933), 245–268.